Controlling the velocity of a femtosecond laser pulse using refractive lenses

Spencer W. Jolly, Olivier Gobert, Antoine Jeandet, Fabien Quéré

Research Article | Vol. 28, No. 4 / 17 February 2020 / Optics Express 4888
Optics EXPRESS

Controlling the velocity of a femtosecond laser pulse using refractive lenses

SPENCER W. JOLLY,[1] OLIVIER GOBERT,[1] ANTOINE JEANDET,[1,2] AND FABIEN QUÉRÉ[1,*]

[1]LIDYL, CEA, CNRS, Université Paris-Saclay, CEA Saclay, 91 191 Gif-sur-Yvette, France
[2]Amplitude Laser Group, Science Business Unit, 91090 Lisses, France
[*]fabien.quere@cea.fr

Abstract: The combination of temporal chirp with a simple chromatic aberration known as longitudinal chromatism leads to extensive control over the velocity of laser intensity in the focal region of an ultrashort laser beam. We present the first implementation of this effect on a femtosecond laser. We demonstrate that by using a specially designed and characterized lens doublet to induce longitudinal chromatism, this velocity control can be implemented independent of the parameters of the focusing optic, thus allowing for great flexibility in experimental applications. Finally, we explain and demonstrate how this spatiotemporal phenomenon evolves when imaging the ultrashort pulse focus with a magnification different from unity.

1. Introduction

Control and manipulation of laser beams has a broad realm of applications in many different fields. Well-known examples of spatial shaping are the Airy beam [1,2] or the Bessel beam [3,4]. For ultrashort laser pulses, such shaping is possible spatio-temporally, i.e. by introducing correlations between the temporal and spatial degrees of freedom of the electric field that are non-separable [5–8]. Here we discuss the so-called flying focus effect whereby the velocity of the light intensity peak formed within the focal region of a broadband laser pulse can be arbitrarily different than the speed of light via very simple spatio-temporal shaping [9,10]. This recently identified effect has many potential scientific applications such as ionization waves of arbitrary velocity [11–13], Raman amplification in a plasma [14], particle acceleration [15], and photon acceleration [16]. The flying focus (also referred to as the "sliding focus") has been demonstrated on a laser system with sub-picosecond duration [10] using a diffractive lens to induce spatio-temporal couplings, a scheme well-suited to the rather narrow spectral width of such a laser. We present here an implementation of this effect more appropriate for femtosecond laser beams, which exploits the chromatic properties of a special lens doublet rather than those of a diffractive lens. A key advantage of this configuration is that the shaping is induced independently of the focusing optic, allowing for more flexibility in applications of this effect.

2. Overview of the flying focus

The flying focus requires the spatio-temporal coupling called pulse-front curvature (PFC) in the near-field. For a collimated beam, a PFC α is defined by a radially varying group delay of $\mathrm{GD}(r) = \alpha r^2$. Such a pulsed beam has a "global" duration (related to the spatially-integrated duration) which we define as $\tau_p = \alpha w_i^2$, with w_i the collimated beam radius. As will be illustrated in this manuscript, the α parameter is useful for optical design, but τ_p is really the key quantity characterizing the spatio-temporal coupling of the beam, which is considered severe when τ_p is much larger than the local Fourier-transform limited duration τ_F of the pulse.

In the spectral domain, this coupling is equivalent to a frequency-varying radius of curvature of the beam spatial phase: the beam wavefront is spatially flat at the central laser frequency

#384512 https://doi.org/10.1364/OE.384512
Journal © 2020 Received 28 Nov 2019; revised 19 Jan 2020; accepted 20 Jan 2020; published 7 Feb 2020

Optics EXPRESS

ω_0, but its curvature $1/R$ varies linearly with the frequency offset $\delta\omega = \omega - \omega_0$ within the bandwidth of the pulse, $1/R = 2c\alpha\delta\omega/\omega_0$ [9]. When such a beam is focused, the spatio-temporal coupling therefore turns into longitudinal chromatism (LC): the best-focus position z_0 varies according to frequency as $z_0(\omega) = 2cf^2\alpha\delta\omega/\omega_0$ (f is the focal length of the focusing optic), or equivalently $z_0(\omega) = \tau_p z_R \delta\omega$ (z_R is the Rayleigh length of the focused beam formed by the central frequency ω_0). As a result, such a beam exhibits an extended frequency-integrated Rayleigh length, $z_R^e/z_R = \tau_p\Delta\omega$, with $\Delta\omega \propto 1/\tau_F$ the spectral width of the broadband beam, and $\tau_p\Delta\omega \gg 1$ defining a strongly coupled beam.

The combination of the longitudinal separation of the frequencies in focus and a frequency-varying arrival time, described by the group delay dispersion (GDD) ϕ_2, produces the flying focus effect where within the extended focal region the intensity peak of the pulse can travel at velocities radically different from c [9–11]. This concept is shown schematically in Figs. 1(a)–1(c) for three snapshots at increasing z position. The case with only temporal chirp in Fig. 1(a) still retains an intensity peak velocity of c, but with both LC and temporal chirp the velocity is different than c. In Fig. 1(b), the shorter wavelengths are focused at greater z and also arrive at later time (corresponding to positive LC and positive chirp), so the intensity peak—which occurs at the confluence of the waist position for a given wavelength and the arrival time of the wavelength at that position—traces a path that has a velocity lower than c. For comparison, the speed of light c can be seen by the dotted arrow, which traces the arrival position of any single color across the snapshots. If the arrival time of the colors (chirp) is reversed by changing the sign of ϕ_2 (e.g. by changing the position of a grating in a compressor or stretcher), then the velocity of the intensity peak becomes greater than c as shown in Fig. 1(c), or even negative depending on the magnitude of the chirp (i.e. backwards propagation, which has already been demonstrated experimentally [10,12]).

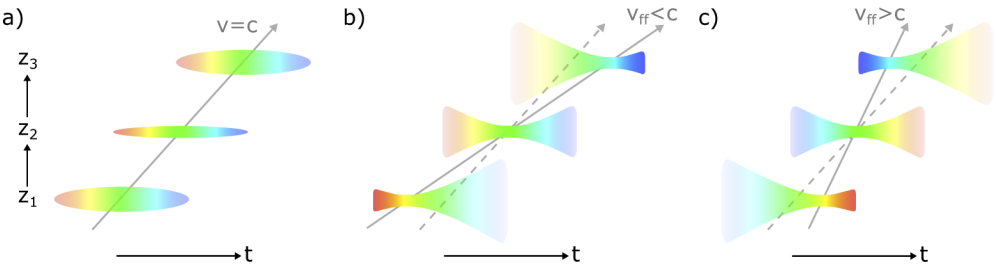

Fig. 1. Conceptual explanation of the flying focus effect. (a) Temporal intensity profile of an ultrashort beam with temporal chirp only, at three positions around the focus. The color code indicates the instantaneous frequency of the pulse, and the brightness its instantaneous intensity. (b) Same representation, now for a beam with both LC and temporal chirp. The velocity of the intensity peak formed by this beam around focus is indicated by the slope of the solid arrow, and is in this case lower than the speed of light (indicated by the slope of the dashed arrow). When the chirp is reversed (c) the flying focus velocity is larger than c.

The expected velocity of the intensity peak was derived in Saint-Marie et al. [9], and is reproduced here:

$$v_{\mathrm{ff}} = \frac{c}{1 + \frac{\phi_2\omega_0}{2\alpha f^2}}, \tag{1}$$

or with the substitutions $\tau_p = \alpha w_i^2$ and $z_R = 2cf^2/\omega_0 w_i^2$:

$$v_{\mathrm{ff}} = \frac{c}{1 + \frac{c\phi_2}{z_R\tau_p}}. \tag{2}$$

Optics EXPRESS

Equation (2) is important for understanding the scaling in a range of scenarios, described in later sections. These relations are a result of simple linear calculations based on the arrival time and waist position of the different frequencies, but more rigorous calculations using the Fourier-transform of the spatio-spectral field agree very well with the simple result [9].

We must note that the flying focus is physically different from the so-called diffraction-free space-time wave packets [17] shown recently to also travel at controllable velocities in free space and in transparent materials [18,19], and to maintain their non-diffractive nature for tens of meters [20,21]. In the flying focus scheme, the velocity different than c is only present within the extended focal region, and although the flying focus has an extended Rayleigh length, there is no diffraction-free nature of the beam outside of this region.

3. Different scenarios for producing the flying focus

Three possible experimental configurations to generate a focused beam with LC are shown in Figs. 2(a)–2(c). The case of Fig. 2(a) uses a diffractive focusing element that inherently focuses different wavelengths to different longitudinal positions. In this case, the effective coupling parameter α is given by $\alpha = 1/2cf$, which produces the relationship $v_{\mathrm{ff}} = c/(1 + \omega_0\phi_2 c/f)$ for the flying focus velocity [10] when the fixed α is inserted in Eq. (1). This results in a limited freedom to control the beam parameters: the coupling parameter α is entirely imposed by the focal length of the diffractive lens at the central frequency. This is quite similar to the very simple case of an ultrashort pulse being focused by a chromatic lens [22], except that the diffractive optic can produce a much larger chromatism.

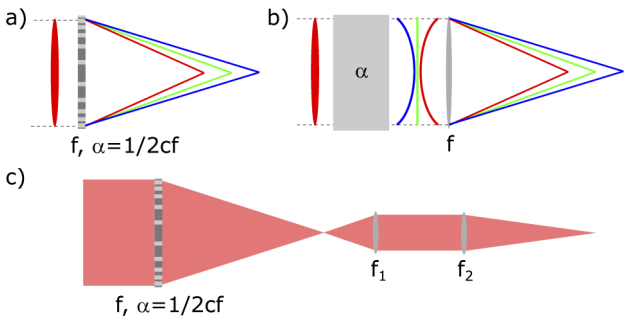

Fig. 2. Production of LC is possible by focusing with a diffractive lens (a), where the spatio-temporal coupling and focal length are related, or by combining an optic that induces PFC on a collimated beam with an achromatic focusing optic (b). In this second case, the induced LC/PFC can be tuned independently from the focal length of the focusing optic. Using a diffractive optic and re-focusing with a different focal length (c) can change the parameters, but restrictions still persist.

In the case of Fig. 2(b), PFC is first induced on the collimated beam by a dedicated chromatic optical system, and the beam is then focused by an independent achromatic focusing optic. This scenario now produces the previous relationship of Eq. (1) [9] where the coupling parameter α and the focal length f are independent of each other. The advantage of this case is that there is more freedom to control all beam parameters. An experiment might require a given waist w_0 in-focus, pulse duration τ in-focus, and v_{ff}, and all of these parameters can be controlled independently via the choice of ϕ_2, f, and α (or equivalently ϕ_2, z_R, and τ_p from the perspective of Eq. (2)). Note especially that α can even be negative in this case, which is not possible with a diffractive lens.

One may imagine that re-focusing a pulse originally focused by a diffractive optic (Fig. 2(c)) may allow for the same flexibility as that in Fig. 2(b), but that is not the case. We will measure and

Optics EXPRESS

discuss the general effect of imaging a flying focus in a later section, albeit using an independent chromatic optical system and not a diffractive lens. This later discussion will explain why there is not increased flexibility in the case of Fig. 2(c).

4. Measurement of the chromatic lens system

In order to generate PFC on the collimated beam in our experiment, we use a doublet consisting of thick lenses of focal length 298 mm and -291 mm (at the central wavelength of 800 nm) composed of glasses S-TIM-2 and PSK53A respectively, separated by a distance of ~ 2 mm in order to essentially act as a telescope (Fig. 3(a)). This combination of one converging and one diverging lens made of different glasses was designed to result in an infinite radius of curvature at the center wavelength of 800 nm (i.e. the beam remains collimated at this wavelength with a magnification close to 1), with as well a minimal spherical aberration. But because the discrepancy between the group velocities of the two glasses is different from that between their phase velocities, the output beam still accrues a quadratically-varying group-delay according to the distance from the center of the lens system, which is exactly PFC, and again precisely equivalent to the imparted curvature depending on frequency. The detailed design of this optic is presented in Sainte-Marie et al. [9], and it is important to note that a doublet of lenses having the same curvature but with the materials exchanged would impart a PFC α of the opposite sign.

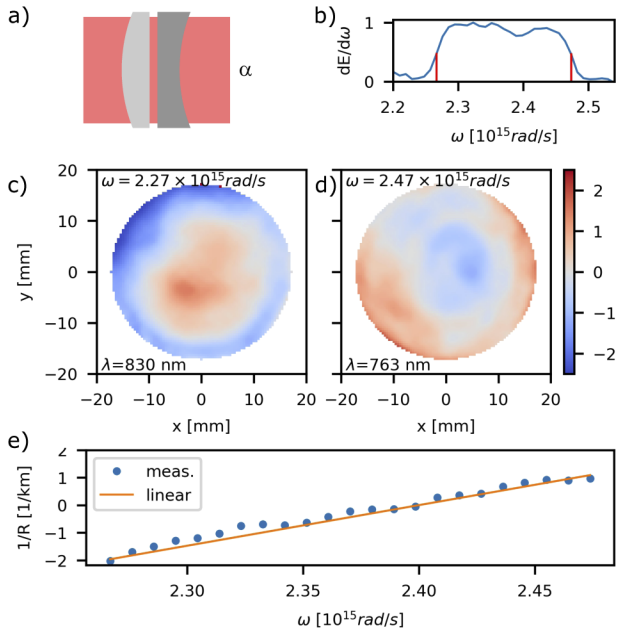

Fig. 3. Creation of PFC on a collimated beam using a chromatic afocal system of lenses made with different glasses, shown in (a). The PFC is characterized using an INSIGHT device, with the measured spatial phase profiles at two frequencies at the edge of the laser bandwidth (frequencies marked in red in (b)) shown in (c–d). The relationship of wavefront curvature to frequency is approximately linear corresponding to a PFC parameter α of 5.9 fs/cm^2, shown in (e).

The effect of the doublet was characterized with an INSIGHT device [23], which provides the complete spatio-spectral properties of the output laser beam in amplitude and phase. We used the ~24 fs pulses delivered by the UHI100 laser source at CEA-Saclay, with a beam apertured to roughly 4 cm diameter in order to avoid clipping in the specific version of the INSIGHT

Optics EXPRESS

device used. The full spectrum is shown in Fig. 3(b) as deduced from the spatial integration of the INSIGHT measurements. Frequency-resolved spatial wavefronts of the beam are shown in Fig. 3(c) and Fig. 3(d), at angular frequencies of 2.27×10^{15} rad/s and 2.47×10^{15} rad/s (830 nm and 762 nm) respectively.

It is clear that the curvature of the beam wavefront is inverted from one extreme of the spectrum to the other. The chromatism is found by calculating the inverse of the radius of curvature at each frequency, related to the Zernike polynomial defocus term, which should be linear in frequency according to $1/R = 2c\alpha\delta\omega/\omega_0$. The design value of the PFC α of 5.9 fs/cm^2 agrees very well with the measured data according to the linear curve shown in Fig. 3(e). This corresponds to a global duration $\tau_p \simeq 95$ fs for a beam of 4 cm radius. Note that this is a much lower value than the PFC produced by the diffractive optic used in Froula et al. [10] with $f = 511$ mm, which amounts to 326 fs/cm^2. Using such PFC values on broadband femtosecond laser pulses would lead to considerable intensity reduction at focus, of the order of 10^{-4} with a 4 cm beam diameter and $\tau_F = 24$ fs, while it is only of the order of 10^{-1} in the scheme presented here.

5. Measurement of the flying focus

We create the flying focus using the full 6.5 cm diameter ($w_i = 3.25$ cm) UHI100 beam. This 100 TW beam was heavily attenuated to ≈ 100 nJ in this instance to avoid any risk of damage to optics or detectors, and focused by an off-axis parabola of focal length $f_0 = 1.1$ m. The experimental schematic can be seen in Fig. 4(a), with the chromatic doublet placed before the large focusing optic, which is displayed as a lens for convenience. Not shown in the schematic are the grating compressor and deformable mirror, both upstream from the experimental area. The grating compressor is used to tune the chirp of the test laser pulse, and the deformable mirror is used to optimize the spatial focal spot (optimized when the doublet is not installed). Note that for experiments at high power, B-integral effects in the doublet would become a major concern in this scheme: since this doublet produces a collimated beam, these could then be avoided by simply moving it before the compressor, into the uncompressed beam (for a small enough α to avoid accumulated spatio-temporal couplings in the compressor).

The first confirmation of the presence of the chromatism imparted on the laser pulses is the comparison between the optimized focal spot with the doublet installed with the full spectrum and only a narrow part of the spectrum in identical conditions, shown in the insets of Fig. 4(b). The spot size in the right inset, where the full bandwidth is present, has increased at the same z position compared to the left inset since not all colors are in best focus with the LC present. This increase of time-integrated beam waist is a characteristic signature of LC in focus [11]. In contrast, it is important to emphasize that for a chirped beam, the instantaneous beam waist at the intensity peak of the beam is not increased compared to the case of the LC-free beam. This is because at any position along the extended Rayleigh length z_R^e, this intensity peak is formed by the fraction of pulse bandwidth that is at its best focus at this particular position.

The flying focus effect is resolved in time by overlapping the test beam with a Fourier-transform-limited probe beam (shown in pink in Fig. 4, but having the same spectrum as the test beam) provided by an independent compressor, and performing spectral interferometry [24] in the focus of the test beam. The spectral interferometry is achieved by placing a 50/50 beamsplitter at the focus of the test beam in the experimental chamber so that the collimated probe beam is overlapped with the focus of the test beam. This plane is then imaged to the slit of an imaging spectrometer with a magnification of $M = 1$, using two achromatic doublet lenses of focal length $f_1 = f_2 = 250$ mm separated by a distance $f_1 + f_2$ (Fig. 4(a)). We discuss in a following section the case when f_2 is increased and the magnification is larger than 1.

The test and probe must have a time delay Δt on the spectrometer slit, shown schematically in Fig. 4(c) along with the spatial format of the two beams on the slit. The intensity on the slit is resolved spectrally, where the spectral interferences will only take place in the region along y

Optics EXPRESS

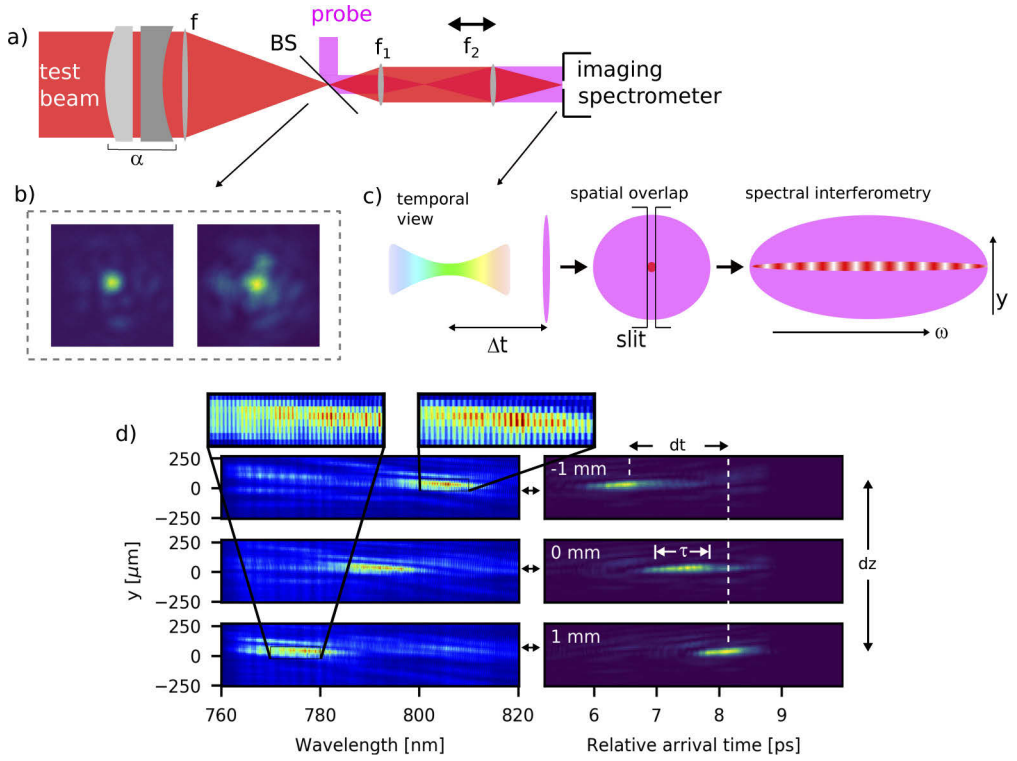

Fig. 4. Experimental setup to induce and measure the flying focus effect (a), drawn with $f_1 = f_2$, with more details in the text, and insets (b) showing the increase in the focal spot size with the doublet installed (left inset: only central wavelength using a bandpass filter, right inset: full bandwidth). The test and probe have a time delay, shown left in (c) along with the format on the spectrometer slit (center) of the two beams and the position of the fringes when dispersed within the spectrometer (right). The analysis procedure involves taking the spectral fringes and Fourier transforming to time. Experimental spectral fringes at three different positions of the last lens are shown on the left in (d), with the insets emphasizing the different fringe spacing, along with the data Fourier transformed to time on the right, showing a velocity different than c. The important measured quantities dt, dz, and τ are shown on the right in panel (d), with dz according to the positions in each subpanel.

where both the test and probe are present. These spectral interferences contain information of the arrival time of the test relative to the probe. This can be seen when analyzing the spectral interferometry signal S between a known probe pulse $\hat{E}_{\text{probe}}$ and a delayed unknown test beam $\hat{E}_{\text{test}}$:

$$\hat{S}(\omega) = \left|\hat{E}_{\text{probe}}(\omega) + \hat{E}_{\text{test}}(\omega)e^{-i(\omega\Delta t)}\right|^2. \tag{3}$$

If the applied delay Δt is large compared to the duration of both pulses, then taking the Fourier transform of $\hat{S}(\omega)$ to go in the time domain, and considering only the peak at positive times, leads to the processed signal:

$$S(t) = \left\{\mathcal{F}_{\omega\to t}\left[\hat{S}(\omega)\right]\right\}_{+\Delta t} \propto E_{\text{probe}}(t) \otimes E_{\text{test}}(t - \Delta t). \tag{4}$$

This corresponds to the convolution of the temporal fields of the probe and test pulses. If the probe pulse is much shorter than the test pulse, then this is a good approximation of the temporal profile of the test pulse. This is the case here, as the probe pulse is close to Fourier-transform limited, while the test pulse is strongly chirped. From this function, we can determine both the

Optics EXPRESS

arrival time of the test pulse relative to the probe (i.e. deviations from the experimental imposed delay Δt, due to the flying focus effect), and its duration (within the approximation specified above). The processed data also has information on the phase of the test beam, but because we are interested in the dynamics of the intensity, we do not include that in the analysis.

We then scan the position of the second imaging lens, and therefore the position z relative to the best focus that is being imaged onto the spectrometer slit. This is not rigorously equivalent to moving the spectrometer through the focal region, but the slight divergence of the probe due to translation of the second lens has a negligible effect on the results. Finally, by calculating the relative arrival time of the test to the probe at different z positions we can deduce the velocity of the intensity of the test beam.

Example results for one chirp setting ($\phi_2 = +20000\,\mathrm{fs}^2$, $M = 3$) are shown in Fig. 4(d). The left panels display raw experimental interferograms (i.e. $\hat{S}(\omega)$) for three different z positions, with the insets showing the different fringe spacing resulting from the variation of the delay between the probe and test beams, due to their different velocities. After Fourier-transforming to time in the right panel of Fig. 4(d) (displaying $|S(t)|^2$), we can see the relative arrival time of the test to the probe for these different z positions deviating from the imposed Δt. Knowing the distance we have moved the lens dz and the change in the relative arrival time dt, the velocity of the intensity peak can be found via the relation

$$v_{\mathrm{ff}} = \frac{c}{1 + c\frac{dt}{dz}}. \tag{5}$$

It is clear that if the arrival time does not change ($dt = 0$), then the test beam is traveling at the same velocity as the probe, c, but if the arrival time varies over z, then the test beam intensity is traveling at a velocity different from c. We note that what we measure here is the velocity of the intensity peak formed by the shaped beam within the Rayleigh range. This is not a phase velocity, but might be considered as some sort of group velocity, with the distinction being rather subtle—as discussed in Section 6 of Sainte-Marie et al. [9].

The results of such velocity measurements are shown in Fig. 5(a), as a function of chirp. The velocities range from $0.77c$ to $2.45c$ and agree relatively well with the prediction of Eq. (1). It is due to the measurement technique that as the velocity becomes larger the calculated velocity will have much more absolute error, even with a fixed error in the measurement of dt (i.e. $\sigma_{v_{\mathrm{ff}}} = v_{\mathrm{ff}}^2 \sigma_{dt}/dz$). The range of ϕ_2 was limited by the spectral resolution of the spectrometer, where at higher chirps information was lost due to the spectral fringe spacing approaching the pixel size.

Using the same processed interferograms as for the velocity calculations, we measure the duration of the intensity peak formed around focus. The results of this analysis for different chirps are displayed as dots in Fig. 5(b), showing durations that always remain below ~2.2 ps for the chirp range investigated here. An interesting and important feature is that the obtained durations are significantly lower than the local duration τ_e of the chirped pulse before focusing, shown as a solid line of Fig. 5(b). This is because for a fixed applied chirp ϕ_2, the duration τ of a pulse increases with its spectral width $\Delta\omega$: $\tau \propto \Delta\omega$ if $\phi_2 \gg 1/\Delta\omega^2$. In the presence of LC in the focal region, the on-axis beam bandwidth $\Delta\omega' \propto 1/\tau_p$ is reduced compared to the full spectral width $\Delta\omega \propto 1/\tau_F$ of the initial beam—an effect that is clearly observed in the spectral data of Fig. 4(d). As a result, the local pulse duration is also reduced compared to τ_e by a factor $\Delta\omega/\Delta\omega' = \tau_p/\tau_F = 2.6$ ($\alpha w_i^2/\tau_F = 5.9 \times 3.25^2/24 = 2.6$). This agrees well with the measurement results in our case (dashed line in Fig. 5(b)). This shorter *local* duration within the focal region, compared to the duration of the unfocused chirped pulse, is a key characteristic signature of the flying focus effect [9,11].

Optics EXPRESS

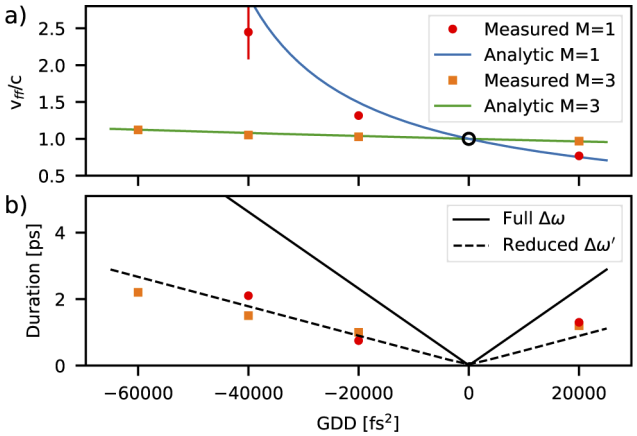

Fig. 5. Results of velocity (a) and pulse duration (b) measurements as a function of chirp, for two different magnifications of the imaging system (see text), $M = 1$ and $M = 3$. The analytic relationships from Eqs.(1)–(2) are shown as lines for each case in (a). The lines in (b) are based on the bandwidth corresponding to $\tau_F = 24$ fs (solid) and the corresponding bandwidth reduced by a factor of 2.6 (dashed).

6. The effect of magnification

We finally investigate how the velocity of the flying focus evolves when imaging the beam focus with different magnifications. To this end, we change the focal length of the second imaging lens in the experimental setup of Fig. 4 to $f_2 = 750$ mm (along with the spacing of the lenses in the telescope), leading to a magnification $M = f_2/f_1 = 3$ from the focus of the parabola to the entrance slit of the spectrometer, instead of $M = 1$ in the previous measurements. The intensity peak velocity and duration measured as a function of chirp in this case are displayed in Fig. 5 as orange squares. The obtained velocities are now very different from the ones obtained for $M = 1$, while the measured durations remain unchanged.

Measuring different velocities when using different magnifications can appear somewhat unexpected, since the only operation between the first focus and the measurement position is simple imaging, which does not affect the pulse velocity when applied to standard pulsed beams. The present case is however different: as shown in Sainte-Marie et al. [9], there is no causality relation between the intensity peaks formed by the focused LC beam along the extended Rayleigh length. In other words, the intensity peak forming at position $z_2 > z_1$ is actually not the result of the propagation of the peak occurring earlier at position z_1. As a result, there is no reason to expect the peak velocity to be conserved upon imaging.

The evolution of the beam properties upon imaging can be derived from analytical calculations, but can also be inferred from simple intuitive considerations. The starting point is that upon imaging by an achromatic stigmatic optical system, the global duration τ_p of the pulse should be conserved. To see how this affects the intensity peak velocity, one can look directly at Eq. (2). By changing the focal length f_2 of the last lens in our experiment, we change the Rayleigh length z_R in the focal region at the spectrometer while keeping τ_p fixed, thus changing in turn the flying focus velocity. The measured velocities agree well with the prediction based on this understanding, which produces the analytic curve for $M = 3$ in Fig. 5(a). Since τ_p remains unaffected, the local duration at focus is not modified significantly either, as observed experimentally. Another interpretation is that an achromatic afocal system made of two lenses of focal lengths f and f_1, which magnifies a beam by a factor f/f_1, will change the PFC parameter α of a beam from α to $\alpha(f/f_1)^2$. The beam with a larger PFC is then focused by an optic of focal length f_2, which

Optics EXPRESS

produces the same results as the previous explanation when using Eq. (1) with the updated parameters (i.e. α and f become $\alpha(f/f_1)^2$ and f_2 in Eq. (1)).

Returning to the experimental scenario of Fig. 2(c), we can now see why the imaging does not increase the flexibility when using the diffractive lens. This is because, although the focused beam waist w_0 and flying focus velicity v_{ff} will be modified by the imaging geometry, both will be described by the new Rayleigh range. This means that, although re-focusing can produce a different v_{ff} and w_0, they can not be tuned independently from each other. Including the pulse duration in the focus as a constraint, then in the case of Fig. 2(c) only two of the three parameters w_0, τ, and v_{ff} can be chosen. The free parameters are still only ϕ_2 and f (equivalently from the perspective of Eq. (2), z_R and τ_p are related to each other by f, $\tau_p = f/\omega_0 z_R$, and therefore not free parameters).

The conceptual understanding of the imaging of the LC/PFC underscores an important property of spatio-temporal couplings, that when an operation is done on either time or space, the spatio-temporal coupling causes that operation to result in changes in both time and space. In our case this means that v_{ff} in the first focus of Fig. 4(a) can be wildly different than that in the second focus where the measurement takes place. In fact, with a correctly chosen chirp they can even be of opposite sign. This phenomenon is exactly what we measured in Fig. 5(a) with the two different magnifications, albeit within a limited range of velocites. With $M = 1$ the measured velocity was the same as in the first focus, but with $M = 3$ the measured velocity was very different.

7. Conclusion

In conclusion, we have presented the first implementation of the flying focus effect on a femtosecond laser system, demonstrating intensity peaks that travel at velocities up to $2.5c$ in vacuum, while the local pulse duration remains below 2.2 ps. The scheme we have used, based on a chromatic afocal doublet, provides great flexibility for experimental applications of this effect, and can be directly applied to high-power laser systems.

Funding

European Research Council (694596).

Acknowledgments

The authors would like to thank Fabrice Reau for operating the laser system and Sandrine Dubosz Dufrénoy for help with the experimental setup.

Disclosures

The authors declare no conflicts of interest.

References

1. G. A. Siviloglou, J. Broky, A. Dogariu, and D. N. Christodoulides, "Observation of accelerating airy beams," Phys. Rev. Lett. **99**(21), 213901 (2007).
2. N. K. Efremidis, Z. Chen, M. Segev, and D. N. Christodoulides, "Airy beams and accelerating waves: an overview of recent advances," Optica **6**(5), 686–701 (2019).
3. J. Durnin, J. J. Miceli, and J. H. Eberly, "Diffraction-free beams," Phys. Rev. Lett. **58**(15), 1499–1501 (1987).
4. D. McGloin and K. Dholakia, "Bessel beams: diffraction in a new light," Contemp. Phys. **46**(1), 15–28 (2005).
5. S. Akturk, X. Gu, P. Bowlan, and R. Trebino, "Spatio-temporal couplings in ultrashort laser pulses," J. Opt. **12**(9), 093001 (2010).
6. G. Zhu, J. van Howe, M. Durst, W. Zipfel, and C. Xu, "Simultaneous spatial and temporal focusing of femtosecond pulses," Opt. Express **13**(6), 2153–2159 (2005).
7. H. Vincenti and F. Quéré, "Attosecond lighthouses: How to use spatiotemporally coupled light fields to generate isolated attosecond pulses," Phys. Rev. Lett. **108**(11), 113904 (2012).

Optics EXPRESS

8. M. Yessenov, B. Bhaduri, H. E. Kondakci, and A. F. Abouraddy, "Classification of propagation-invariant space-time wave packets in free space: Theory and experiments," Phys. Rev. A **99**(2), 023856 (2019).
9. A. Sainte-Marie, O. Gobert, and F. Quéré, "Controlling the velocity of ultrashort light pulses in vacuum through spatio-temporal couplings," Optica **4**(10), 1298–1304 (2017).
10. D. H. Froula, D. Turnbull, A. S. Davies, T. J. Kessler, D. Haberberger, J. P. Palastro, S.-W. Bahk, I. A. Begishev, R. Boni, S. Bucht, J. Katz, and J. L. Shaw, "Spatiotemporal control of laser intensity," Nat. Photonics **12**(5), 262–265 (2018).
11. J. P. Palastro, D. Turnbull, S.-W. Bahk, R. K. Follett, J. L. Shaw, D. Haberberger, J. Bromage, and D. H. Froula, "Ionization waves of arbitrary velocity driven by a flying focus," Phys. Rev. A **97**(3), 033835 (2018).
12. D. Turnbull, P. Franke, J. Katz, J. P. Palastro, I. A. Begishev, R. Boni, J. Bromage, A. L. Milder, J. L. Shaw, and D. H. Froula, "Ionization waves of arbitrary velocity," Phys. Rev. Lett. **120**(22), 225001 (2018).
13. P. Franke, D. Turnbull, J. Katz, J. P. Palastro, I. A. Begishev, J. Bromage, J. L. Shaw, R. Boni, and D. H. Froula, "Measurement and control of large diameter ionization waves of arbitrary velocity," Opt. Express **27**(22), 31978–31988 (2019).
14. D. Turnbull, S. Bucht, A. Davies, D. Haberberger, T. Kessler, J. L. Shaw, and D. H. Froula, "Raman amplification with a flying focus," Phys. Rev. Lett. **120**(2), 024801 (2018).
15. S. W. Jolly, "Influence of longitudinal chromatism on vacuum acceleration by intense radially polarized laser beams," Opt. Lett. **44**(7), 1833–1836 (2019).
16. A. J. Howard, D. Turnbull, A. S. Davies, P. Franke, D. H. Froula, and J. P. Palastro, "Photon acceleration in a flying focus," Phys. Rev. Lett. **123**(12), 124801 (2019).
17. H. E. Kondakci and A. F. Abouraddy, "Diffraction-free space-time light sheets," Nat. Photonics **11**(11), 733–740 (2017).
18. B. Bhaduri, M. Yessenov, and A. F. Abouraddy, "Space-time wave packets that travel in optical materials at the speed of light in vacuum," Optica **6**(2), 139–146 (2019).
19. H. E. Kondakci and A. F. Abouraddy, "Optical space-time wave packets having arbitrary group velocities in free space," Nat. Commun. **10**(1), 929 (2019).
20. B. Bhaduri, M. Yessenov, and A. F. Abouraddy, "Meters-long propagation of diffraction-free space-time light-sheets," Opt. Express **26**(16), 20111–20121 (2018).
21. B. Bhaduri, M. Yessenov, D. Reyes, J. Pena, M. Meem, S. R. Fairchild, R. Menon, M. Richardson, and A. F. Abouraddy, "Broadband space-time wave packets propagating 70 m," Opt. Lett. **44**(8), 2073–2076 (2019).
22. Z. Bor, "Distortion of femtosecond laser pulses in lenses," Opt. Lett. **14**(2), 119–121 (1989).
23. A. Borot and F. Quéré, "Spatio-spectral metrology at focus of ultrashort lasers: a phase-retrieval approach," Opt. Express **26**(20), 26444–26461 (2018).
24. L. Lepetit, G. Chériaux, and M. Joffre, "Linear techniques of phase measurement by femtosecond spectral interferometry for applications in spectroscopy," J. Opt. Soc. Am. B **12**(12), 2467–2474 (1995).